MOLECULAR AND CELLULAR BIOLOGY, July 2011, p. 2920–2933 Vol. 31, No. 14
0270-7306/11/$12.00 doi:10.1128/MCB.05431-11

Mammalian *Llgl2* Is Necessary for Proper Branching Morphogenesis during Placental Development[▽]

Smitha Sripathy,[1] Minhui Lee,[1] and Valeri Vasioukhin[1,2]*

Division of Human Biology, Fred Hutchinson Cancer Research Center, Seattle, Washington 98109,[1] and Department of Pathology and Institute for Stem Cell and Regenerative Medicine, University of Washington, Seattle, Washington 98195[2]

Received 30 March 2011/Returned for modification 20 April 2011/Accepted 11 May 2011

Cell polarity plays a critical role in the development of all metazoans; however, the mechanisms of cell polarity and the specific role of cell polarity pathways in mammalian organisms are still poorly understood. Lethal giant larvae (*Lgl*) is an apical-basal polarity gene identified in *Drosophila*, where it functions as a tumor suppressor controlling self-renewal and differentiation of progenitor cells. There are two orthologs of *Lgl* in mammalian genomes: *Llgl1* and *Llgl2*. While mammalian *Lgls* are assumed to be tumor suppressor genes, little is known about their function *in vivo*. Here we report the functional analysis of murine *Llgl2*. We generated *Llgl2*$^{-/-}$ mice and found that Llgl2 functions as a polarity protein required for proper branching morphogenesis during placental development. *Llgl2*$^{-/-}$ pups are born as runts but quickly catch up in size and grow into normal-size adults. Surprisingly, no prominent phenotypes or spontaneous tumors were observed in adult *Llgl2*$^{-/-}$ mice. Analyses of placental trophoblasts reveal a critical role for *Llgl2* in cell polarization and polarized cell invasion. We conclude that mammalian *Llgl2* is required for proper polarized invasion of trophoblasts and efficient branching morphogenesis during placental development, but, unlike its *Drosophila* ortholog, it does not function as a canonical tumor suppressor gene.

Cell polarity and cell-cell adhesion play a critical role in the regulation of normal tissue architecture and function. Disruption of cell adhesion and cell polarity is often associated with neoplastic tumors (4, 19). *Lgl* (lethal giant larvae) is the first described *Drosophila* tumor suppressor gene, originally discovered by Bridges in the 1930s and further characterized in modern times by Elisabeth Gateff and Bernard Mechler (10–12, 23). Subsequent functional analysis revealed that Lgl is a polarity protein that is required for apical-basal polarization and asymmetric cell division of *Drosophila* neuroblasts (27, 29, 30). *Lgl* mutant progenitors are unable to generate daughter cells that completely withdraw from the cell cycle and differentiate. Instead, they produce progenitors that continue to divide, overproliferate, and kill the animals, exhibiting a phenotype which is remarkably similar to cancer in mammalian organisms (26). Similarly to neuronal tissues, epithelial cells also hyperproliferate in *Lgl* mutant *Drosophila* larvae (5).

The potential role of stem cells in cancer initiation in mammalian organisms is a hotly debated topic of modern cancer biology. Since *Drosophila Lgl* is involved in regulation of stem cell self-renewal and loss of *Lgl* in *Drosophila* causes stem cell-derived tumors, it is plausible that mammalian orthologs of *Lgl*, *Llgl1*, and *Llgl2* are also involved in regulation of stem cell self-renewal and function as tumor suppressors. Indeed, the human *Llgl1* can rescue the phenotype of *Lgl*-mutant *Drosophila*, indicating the conservation of Lgl function across species (14, 15). We have previously reported that *Llgl1*$^{-/-}$ mice develop severe brain dysplasia and die at birth from massive hydrocephalus (18). The role of mammalian *Llgl2* remained unknown; however, *Llgl2*-mutant zebrafish (*penner* mutation) are unable to form hemidesmosomes and display hyperproliferation and disorganization of the basal epidermis (40, 41). While *pen*/*Llgl2* mutants die at 4 to 5 days postfertilization, transplantation of *Llgl2*$^{-/-}$ cells into normal fish embryos results in development of epidermal tumors, a phenotype that enabled the authors to identify vertebrate *Llgl2* as a tumor suppressor gene (31).

To investigate the role of mammalian *Llgl2 in vivo*, we generated and analyzed *Llgl2*$^{-/-}$ mice. We found that *Llgl2* is required for proper placental development. *Llgl2*$^{-/-}$ pups are born as runts but quickly catch up in size to control littermates and display no overt phenotypes throughout their subsequent life. Hemidesmosomes are formed and functional, and there is no hyperplasia or tumor development in *Llgl2*$^{-/-}$ mice. Analysis of the placental defects revealed an important role of *Llgl2* in polarized invasion of trophoblasts and branching morphogenesis of the placental labyrinth layer. We conclude that murine *Llgl2* is required for proper polarization of trophoblast cells during placental morphogenesis but plays a redundant function in the adult organism. Loss of *Llgl2* does not predispose mice to spontaneous tumor development, indicating that mammalian *Llgl2* is not a canonical tumor suppressor gene.

MATERIALS AND METHODS

Generation of *Llgl2*$^{-/-}$ mice and genotyping. A mutation was generated in the *Llgl2* gene via insertion of the gene trap vector pGT0lxf into the intron immediately downstream from the exon with the first ATG site (clone no. XS0846; SIGTR). Chimeric mice were generated using standard ES cell technology (16a). Heterozygous *Llgl2*$^{tm2Vv+/-}$ mice were crossed to C57BL/6J mice for eight generations and were subsequently interbred to obtain homozygous mutant B6.129P2-*Llgl2*$^{tm2Vv-/-}$ mice. The mutant mice were genotyped using PCR analysis with 5-CGCCATACAGTCCTCTTCAC-3, 5-CTGCACACTGCGGATTTAGC-3, and 5-CAGCTCTGGGCCTTTTTCAC-3 oligonucleotides, which produce a PCR fragment of 200 bp for the wild type and 350 bp for the mutant allele.

* Corresponding author. Mailing address: Division of Human Biology, Fred Hutchinson Cancer Research Center, Seattle, WA 98109. Phone: (206) 667-1710. Fax: (206) 667-6524. E-mail: vvasiouk@fhcrc.org.

▽ Published ahead of print on 23 May 2011.

Histology, immunohistochemistry, and electron microscopy. Freshly collected tissues were fixed overnight in 4% paraformaldehyde, dehydrated in increased concentrations of ethanol, cleared with xylene, and embedded in paraffin. Sections (4 μm) of the paraffinized blocks were made close to the placental midline and stained with hematoxylin and eosin. For immunohistochemistry, tissue sections were rehydrated and stained with anti-Ki67 (Novo Castra), anti-phosphohistone H3 (Cell Signaling), anti-β-catenin (Sigma), anti-PKCzeta (Santa Cruz), anti-connexin 26 (gift from Paul Lampe, FHCRC), anti-β4-integrin (gift from William Carter, FHCRC), or antilaminin (Sigma) antibodies. Anti-E-cadherin antibodies were generated in rabbits by using a glutathione *S*-transferase (GST)–cytoplasmic-E-cadherin fusion containing the C-terminal 145 amino acids of canine E-cadherin (GB no. XM_536807.2) (Strategic Biosolutions). The antigens were detected using Vectastain ABC kit (Vector Labs) according to manufacturers' specifications. Terminal deoxynucleotidyltransferase-mediated dUTP-biotin nick end labeling (TUNEL) stainings were performed using the ApopTag Plus peroxidase kit (Millipore) per the manufacturer's instructions. For immunofluorescent stainings, the primary antibodies were detected using corresponding Texas Red or fluorescein isothiocyanate (FITC)-labeled secondary antibodies (Jackson Lab Immunoresearch). Placental endogenous alkaline phosphatase activity was detected as described previously (33). Stained slides were examined and photographed using an Olympus BX41 microscope and Microfire camera (Optronics) or a Zeiss LSM 510 confocal microscope. To determine the placental labyrinth layer transport surface area, we performed a morphometric analysis of the alkaline phosphatase-positive cells (44). For transmission electron microscopy (EM), samples were fixed in Karnoy's fixative for 2 days at 4°C and processed for Epon embedding. Sections were made close to the placental midline and analyzed with a JEOL 1010 microscope. Digital images were pseudocolored using Adobe Photoshop software.

***In situ* hybridization.** The plasmids used for synthesis of sense and antisense *Llgl2* probes have been previously described (18). Labeled RNA probes were generated using a digoxigenin (DIG) RNA labeling kit (Roche). Frozen sections (14 μm) were rehydrated in phosphate-buffered saline (PBS) and postfixed with 4% paraformaldehyde, treated with proteinase K (1 μg/ml for 15 min at room temperature), acetylated (1 min at room temperature), and hybridized with labeled probes overnight at 58°C. Hybridization buffer contained 0.3 mg/ml yeast tRNA (Sigma-Aldrich), 5× SSC (1× SSC is 0.15 M NaCl plus 0.015 M sodium citrate) (Ambion), 50% formamide, 5× Denhardt's solution (Sigma-Aldrich), 20 mM dithiothreitol (DTT), 0.1% (vol/vol) herring sperm DNA (Sigma-Aldrich), and DIG-labeled RNA probe (5% of the transcription reaction from 1 μg template DNA). After hybridization, slides were first washed with 5× SSC buffer and 2× SSC buffer at 70°C and then with 0.2× SSC buffer at room temperature and then treated with blocking buffer (Roche) for 1 h at room temperature. Slides were then incubated in a 1:200 dilution of horseradish peroxidase (HRP)-conjugated anti-DIG antibody (Roche) for 1 h, washed, and incubated for 10 min with TSA-biotin (Perkin-Elmer). The probes were detected by incubating with a 1:2,000 dilution of streptavidin-Alexa 488 (Molecular Probes) and the cell nuclei were counterstained with DAPI (4′,6-diamidino-2-phenylindole).

RNA extraction and quantitative reverse transcription-PCR (qRT-PCR). Total RNA was extracted using TRIZOL (Invitrogen), and cDNA was prepared using the Superscript III first-strand synthesis kit (Invitrogen). Quantitative PCR (qPCR) was performed using Prism 7900HT (Applied Biosystems), platinum qPCR mix (Invitrogen) and the Universal Probe Library kit utilizing the primers, probes, and PCR conditions recommended by the Universal Probe Library assay center (Roche Applied Science). Ribosomal protein Rps16 was used for normalization of qPCR data.

Cell culture and lentivirus production. The SM10 mouse placental labyrinth trophoblast cells were a gift from Joan Hunt (University of Kansas) and were maintained in RPMI 1650 medium supplemented with 10% fetal bovine serum (FBS), 2 mM glutamine, 50 μM 2-mercaptoethanol, and 1 mM sodium pyruvate. Human embryonic kidney (HEK) 293FT cells (Invitrogen) were grown in 5% CO_2 in Dulbecco's modified essential medium containing 10% FBS and antibiotics. The lentiviruses were produced in HEK293FT cells as described previously (22). The SM10 cells were infected with short hairpin RNA (shRNA) lentiviruses, and stably transduced cells were fluorescence-activated cell sorter (FACS) sorted for green fluorescent protein (GFP) expression. To overexpress human LLGL2, SM10 cells were infected with pLenti6 lentiviruses carrying either lacZ-V5 or hLLGL2-V5 constructs. Stably transduced cells were generated by selection with 3 μg/ml of blasticidin.

DNA constructs. Full-length human LLGL2 cDNA was PCR amplified from IMAGE clone 3584689 and cloned into the Gateway pCR8/GW/TOPO entry clone (Invitrogen). A lentiviral construct encoding C-terminal V5-tagged human *LLGL2* was generated by an LR Gateway reaction from the entry clone into pLenti6/V5-DEST (Invitrogen). Control pLenti6/V5-GW/LacZ vector was obtained from Invitrogen. Lentiviral shRNA construct targeting mouse *Llgl2* was generated by inserting 5-GGATCCGGAAGAGAGGTTCACATTGCTTCAA GAGAGCAATGTGAAGCTCTCTTCTTTTTGGAATTC-3 oligonucleotide into BamHI and EcoRI sites of FUGW-H1-GFP-neomycin vector (21).

Western blot analysis and zymography. Tissues were homogenized and cultured cells were lysed in ice-cold lysis buffer containing 1 mM EDTA, 1 mM EGTA, and 1% Triton X-100 in PBS, along with complete protease and phosphatase inhibitor tablets (Roche). The lysates were centrifuged at 13,000 × *g* for 10 min at 4°C, and the supernatants were used for Western blot analysis. Protein samples were separated on NuPAGE gradient gels (Invitrogen), transferred to polyvinylidene difluoride (PVDF) membranes (Millipore), and analyzed by Western blotting with anti-human LLGL2 (Abcam), antitubulin (University of Iowa Hybridoma Bank) and β-actin (Sigma), anti-mouse Llgl1 (18), and anti-mouse Llgl2 antibodies. Anti-mouse Llgl2 antibodies were produced in rabbits against the GST fusion containing amino acids 933 to 1027 of mouse Llgl2 (GB no. NM_145438.2) and purified by affinity chromatography. Protease zymography was performed using Novex 10% gelatin gels and protein renaturation and developing buffers as recommended by the manufacturer (Invitrogen). Protease activity was detected by staining with a colloidal blue kit (Invitrogen).

Matrigel invasion and migration assays. Matrigel invasion and cell migration assays were performed using an 8-μm BD BioCoat Matrigel invasion chamber and cell culture inserts, as described by the manufacturer (BD Biosciences). Cells were plated into the Matrigel invasion chamber or cell culture inserts in the presence of growth medium lacking FBS. Medium containing 10% FBS was used in the lower chamber as a chemoattractant. Cells were allowed to migrate/invade across the membrane for 8 or 24 h, and migrated cells were stained with a DIFF stain kit (IMEB Inc.) per the manufacturer's instructions. Cells at four edges and at the center of each membrane were imaged, and the number of migrated cells was counted using Image J software. The percentage of cell invasion was determined as specified by the manufacturer.

Quantitation of cell polarization. Scratch wound cell polarization assays were performed as previously described (36). Cell polarization induced by wounding was determined 1 h after scratching an 80% confluent cell monolayer. Cells were fixed and stained with antipericentrin antibodies (Covance) and DAPI nuclear counterstain. The first row of cells showing the centrosome located in front of the nucleus and the first row in the 120° sector facing the wound were counted as oriented; ≥150 cells were counted per coverslip, with four independent experiments per each data point. Statistical tests were performed using a two-tailed *t* test with equal variances.

RESULTS

Generation of *Llgl2*$^{-/-}$ mice. To investigate the role of *Llgl2 in vivo*, we generated and analyzed *Llgl2*$^{-/-}$ mice (Fig. 1). The *Llgl2* gene was modified in ES cells by the insertion of a retroviral gene trap vector containing strong splice acceptor, β-geo, and polyadenylation sequences (Fig. 1A). The gene trap sequences were inserted into the second intron, immediately downstream from the exon encoding the first methionine and 25 N-terminal amino acids of Llgl2. In the targeted gene configuration, the Llgl2 transcript would terminate with the β-geo polyadenylation sequences and exon 2 of *Llgl2* would be spliced with β-geo coding sequence, effectively generating the *Llgl2*-null allele. ES cell technology was used to generate the *Llgl2*$^{+/-}$ mice. To obtain pure genetic background, the heterozygous *Llgl2*$^{+/-}$ animals were crossed for eight generations to C57BL/6J mice. The resulting *Llgl2*$^{+/-}$ mice were crossed to each other to obtain homozygous mutant *Llgl2*$^{-/-}$ mice. Western blot analysis with antibodies recognizing murine Llgl2 demonstrated the absence of Llgl2 protein in *Llgl2*$^{-/-}$ mice (Fig. 1B). In addition, we did not observe the formation of truncated Llgl2 protein fragments in *Llgl2*$^{-/-}$ tissues, confirming generation of *Llgl2* knockout mice (see Fig. 4A).

Growth retardation of *Llgl2*$^{-/-}$ embryos and neonatal pups but normal size of adult *Llgl2*$^{-/-}$ mice. *Llgl2*$^{-/-}$ newborns were smaller than their wild-type and heterozygous littermates, and many did not survive to weaning (Fig. 1C). Surprisingly,

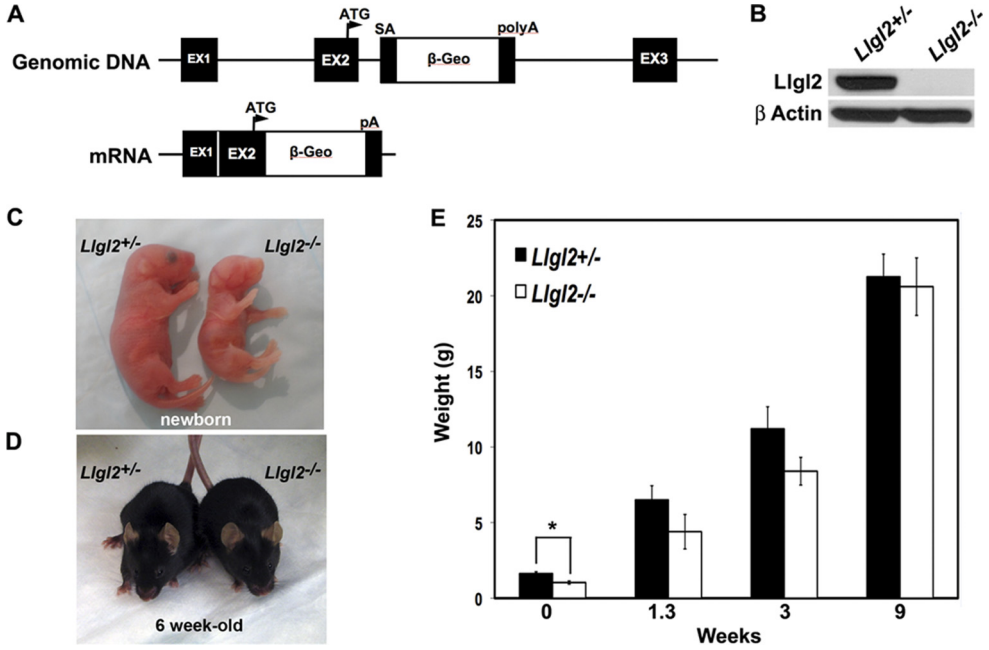

FIG. 1. Generation and embryonic growth retardation phenotype of *Llgl2*$^{-/-}$ mice. (A) Schematic representation of gene trap-targeted *Llgl2* allele (genomic DNA), and the predicted resulting transcript (mRNA). ATG, the initiating methionine in exon 2. SA, strong splice acceptor. polyA, strong polyadenylation site. (B) Western blot analyses of kidney protein extracts from *Llgl2*$^{-/-}$ and *Llgl2*$^{+/-}$ newborn animals. The blot was analyzed with anti-Llgl2 and anti-β-actin antibodies. (C) Gross appearance of newborn *Llgl2*$^{-/-}$ and *Llgl2*$^{+/-}$ littermates. Note that *Llgl2*$^{-/-}$ newborns are significantly smaller than their heterozygous and wild-type littermates. (D) Gross appearance of adult (6-week-old) *Llgl2*$^{-/-}$ and *Llgl2*$^{+/-}$ littermates. Note that *Llgl2*$^{-/-}$ adults are indistinguishable from their control littermates. (E) Differences in weight between *Llgl2*$^{-/-}$ and *Llgl2*$^{+/-}$ littermates. Graph shows the weights of the pups at the indicated time points after birth. Error bars represent standard deviations. Note that significant differences in weight in newborn pups quickly disappear after birth.

pups that did survive to weaning quickly caught up with their littermates and grew to be normal-sized adults (Fig. 1D and E). Also, reducing the size of the litters containing *Llgl2*$^{-/-}$ newborns eliminated perinatal death of *Llgl2*$^{-/-}$ pups, indicating that competition for milk with larger siblings was responsible for their death. Histological examination of major organs from adult *Llgl2*$^{-/-}$ mice did not reveal any significant abnormalities in these animals (data not shown). This was unexpected, because *Lgl2*$^{-/-}$ zebrafish display a prominent epidermal phenotype and die within a few days postfertilization. Mutant fish are unable to form hemidesmosomes, which are prominent cell-substratum adhesion structures connecting epidermis with the basement membrane. Ablation of hemidesmosomes in mice results in a dramatic skin-blistering phenotype and neonatal lethality (7). Hence, we analyzed skins of newborn *Llgl2*$^{-/-}$ pups by histology and staining for hemidesmosomal marker integrin-β4 and found normal hemidesmosomes and overall skin morphology in *Llgl2*$^{-/-}$ mice (Fig. 2). These data indicate that, unlike zebrafish *Lgl2*, murine *Llgl2* is not required for hemidesmosome formation and function.

To reveal whether adult phenotypes in *Llgl2*$^{-/-}$ mice will become apparent with age, we monitored *Llgl2*$^{-/-}$ mice up to 2 years of age; however, no prominent phenotype developed in these animals ($n = 9$). Both male and female *Llgl2*$^{-/-}$ mice were fertile. We conclude that *Llgl2* is important for proper embryonic development but is not essential in adult mice.

Placental defects in *Llgl2*$^{-/-}$ embryos. Since *Llgl2*$^{-/-}$ newborns are born as runts but catch up in size by adulthood, we hypothesized that placental defects may be responsible for the growth retardation of *Llgl2*-mutant embryos. We measured the weights of both embryos and placentas between embryonic day 11.5 (E11.5) and E18.5 (Fig. 3A and B). Consistent with our hypothesis, we found that the differences in weights between

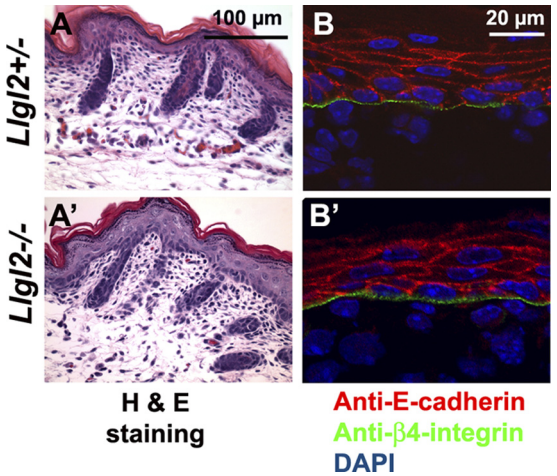

FIG. 2. Normal histology and deposition of hemidesmosomes in the skins of *Llgl2*$^{-/-}$ pups. (A and A′) Hematoxylin and eosin (H & E) staining of sagittal sections through the back skin of newborn *Llgl2*$^{-/-}$ and *Llgl2*$^{+/-}$ pups. (B and B′) Immunofluorescent staining of newborn skin sections from *Llgl2*$^{-/-}$ and *Llgl2*$^{+/-}$ pups with anti-E-cadherin (adherens junction marker, red) and anti-β4-integrin (hemidesmosome marker, green) antibodies. Blue is a DAPI nuclear counterstain.

Llgl2$^{+/-}$ and *Llgl2*$^{-/-}$ placentas preceded the differences in weights between the embryos. E15.5 was the earliest time point when a difference in the weights of *Llgl2*$^{+/-}$ and *Llgl2*$^{-/-}$ embryos was observed (Fig. 3A). However, *Llgl2*$^{-/-}$ placentas were smaller than *Llgl2*$^{+/-}$ placentas as early as E12.5 (Fig. 3B). Murine placenta contains maternal decidua and three principal placental layers: the outer layer of trophoblast giant cells, the middle layer of spongiotrophoblasts, and the innermost labyrinth layer containing highly branched blood vessels used for the exchange of nutrients between the mother and the embryo (43). To analyze potential placental defects in more detail, we performed histological analysis of *Llgl2*$^{-/-}$ and *Llgl2*$^{+/-}$ placentas at E11.5 to E14.5 (Fig. 3C to F). As expected, *Llgl2*$^{-/-}$ placentas were smaller in size than placentas from *Llgl2*$^{+/-}$ and wild-type animals. Interestingly, the area of the *Llgl2*$^{-/-}$ labyrinth layer was significantly decreased, while the areas of the spongiotrophoblast and trophoblast giant cell layers were not changed (Fig. 3G). Since *Llgl2*$^{-/-}$ females are fertile, we also analyzed *Llgl2*$^{-/-}$ placentas from embryos carried by *Llgl2*$^{-/-}$ mothers. However, we did not find differences between these placentas and *Llgl2*$^{-/-}$ placentas from embryos carried by *Llgl2*$^{+/-}$ mothers, indicating that maternal Llgl2 does not play an important role in placental development (data not shown). Our data indicate that murine *Llgl2* is important for the proper development of the placental labyrinth cell layer.

We next analyzed the expression pattern of *Llgl2* in mouse placenta. Western blot analysis revealed a complete loss of Llgl2 protein in *Llgl2*$^{-/-}$ placentas (Fig. 4A). Llgl1 was expressed at low levels in wild-type placentas, and its levels were not upregulated in *Llgl2*$^{-/-}$ mutants (Fig. 4A). Our anti-Llgl2 antibodies were unsuitable for immunohistochemical (IHC) staining; therefore, we used *in situ* hybridization with an *Llgl2* antisense probe to analyze the expression pattern of *Llgl2* in mouse placenta. We found that *Llgl2* is prominently expressed in the labyrinth layer and shows very low levels of expression in the maternal decidual layer (Fig. 4B). *Llgl2*$^{-/-}$ placentas were used as negative controls to confirm specificity of the *in situ* hybridization (Fig. 4B). As an alternative approach, we performed X-Gal (5-bromo-4-chloro-3-indolyl-β-D-galactopyranoside) stainings of placental sections for β-geo expression, which was controlled by the endogenous *Llgl2* promoter. While wild-type placentas did not stain for LacZ, *Llgl2*$^{-/-}$ placentas displayed prominent LacZ staining in the trophoblasts of the labyrinth layer (Fig. 4C). Therefore, we conclude that *Llgl2* is prominently expressed in the trophoblasts of the labyrinth cell layer, which is defective in *Llgl2*$^{-/-}$ placentas.

The smaller size of the *Llgl2*$^{-/-}$ labyrinth cell layer could potentially be due to decreased cell proliferation or increased cell death in the *Llgl2*$^{-/-}$ placenta. To analyze cell proliferation, we performed IHC with anti-phospho-histone H3 (mitotic cell marker) and anti-Ki67 (cell proliferation marker) antibodies (Fig. 5A and D). No significant differences were detected in the rates of cell proliferation, either in the *Llgl2*$^{-/-}$ labyrinth or in the spongiotrophoblast cell layer, compared to controls (Fig. 5B, C, E, and F). To analyze the programmed cell death, we performed TUNEL staining on E13.5 and E15.5 placentas from *Llgl2*$^{-/-}$ and *Llgl2*$^{+/-}$ mice (Fig. 5G). No significant differences were observed in the number of apoptotic cells between the *Llgl2*$^{-/-}$ and *Llgl2*$^{+/-}$ placentas (Fig. 5H). We conclude that ablation of *Llgl2* does not result in significant changes in placental cell proliferation or apoptosis.

***Llgl2* is required for proper branching morphogenesis during development of the placental labyrinth layer.** The labyrinth cell layer is formed by extensive branching morphogenesis of the villi, which are generated by fetal trophoblasts and contain fetal endothelial blood vessels. Villi are bathed in the maternal blood, and extensive branching tremendously increases the transport surface area of the villi, which are used to exchange oxygen and nutrients between the maternal and embryonic blood. The trophoblast cells on the surface of the villi line the maternal blood spaces. As these cells express endogenous alkaline phosphatase, the staining for alkaline phosphate activity is routinely used to distinguish the maternal lumens and to measure both the extent of branching and the transport surface area of the labyrinth (1, 44). Alkaline phosphatase staining of E13.5 and E14.5 *Llgl2*$^{-/-}$ and *Llgl2*$^{+/-}$ placentas revealed an increase in the size of maternal blood lumens and a decrease in the trophoblast transport surface area in the labyrinth of *Llgl2*$^{-/-}$ placentas (Fig. 6A to C). In E13.5 *Llgl2*$^{+/-}$ placentas, ~54% of the maternal blood lumens are small (0.5 to 5 pixels) and only ~6% are large (20 to 200 pixels), indicating a well-branched labyrinth (Fig. 6B). In contrast, in E13.5 *Llgl2*$^{-/-}$ placentas, only ~30% of the maternal lumens are small (0.5 to 5 pixels) and ~28% are large (20 to 200 pixels), indicating inefficient branching morphogenesis in the labyrinth layer. Alkaline phosphatase stainings of placental sections at E11.5 did not reveal significant differences in branching, indicating that the branching deficiency is not apparent at the early stages of placental development (data not shown).

The fetal blood vessels develop within the branched villi. These vessels are lined by endothelial cells, which are connected to the laminin-rich basement membrane separating the endothelial and trophoblast cell layers. Hence, staining for laminin is routinely used to reveal the embryonic blood lumens (44). Analyses of fetal blood lumen sizes and surface areas using staining with antilaminin antibodies revealed an increase in fetal lumen size and a decrease in the surface area of fetal blood vessels at E13.5 and E14.5, but not at E11.5 in *Llgl2*$^{-/-}$ placentas (Fig. 7 and data not shown). Embryonic vessels are limited to the villi, which are generated by branching morphogenesis of the fetal trophoblasts. Hence, the observed decrease in surface area and increase in size of the embryonic blood spaces are indicative of a secondary defect rather than a primary vascularization defect in *Llgl2*$^{-/-}$ placentas. We conclude that *Llgl2* is required for proper branching morphogenesis executed by fetal trophoblasts during development of the mouse placental labyrinth layer.

Formation of trilaminar layer in *Llgl2*$^{-/-}$ placentas. To further characterize the defects in the *Llgl2*$^{-/-}$ labyrinth layer, we analyzed the interface between the maternal and fetal blood lumens using electron microscopy. In mouse placenta, fetal vessels and maternal blood lumens are separated by a trilaminar trophoblast layer, consisting of a bilayer of syncytiotrophoblasts surrounding the fetal blood vessel and a single layer of mononuclear trophoblasts lining the maternal sinuses (Fig. 8A and B) (43). The syncytiotrophoblast layers I and II (STI and STII) are formed as a result of cell-cell and cell-syncytium fusion events and tightly adhere to each other. They constitute the site of nutrient and gaseous exchange between

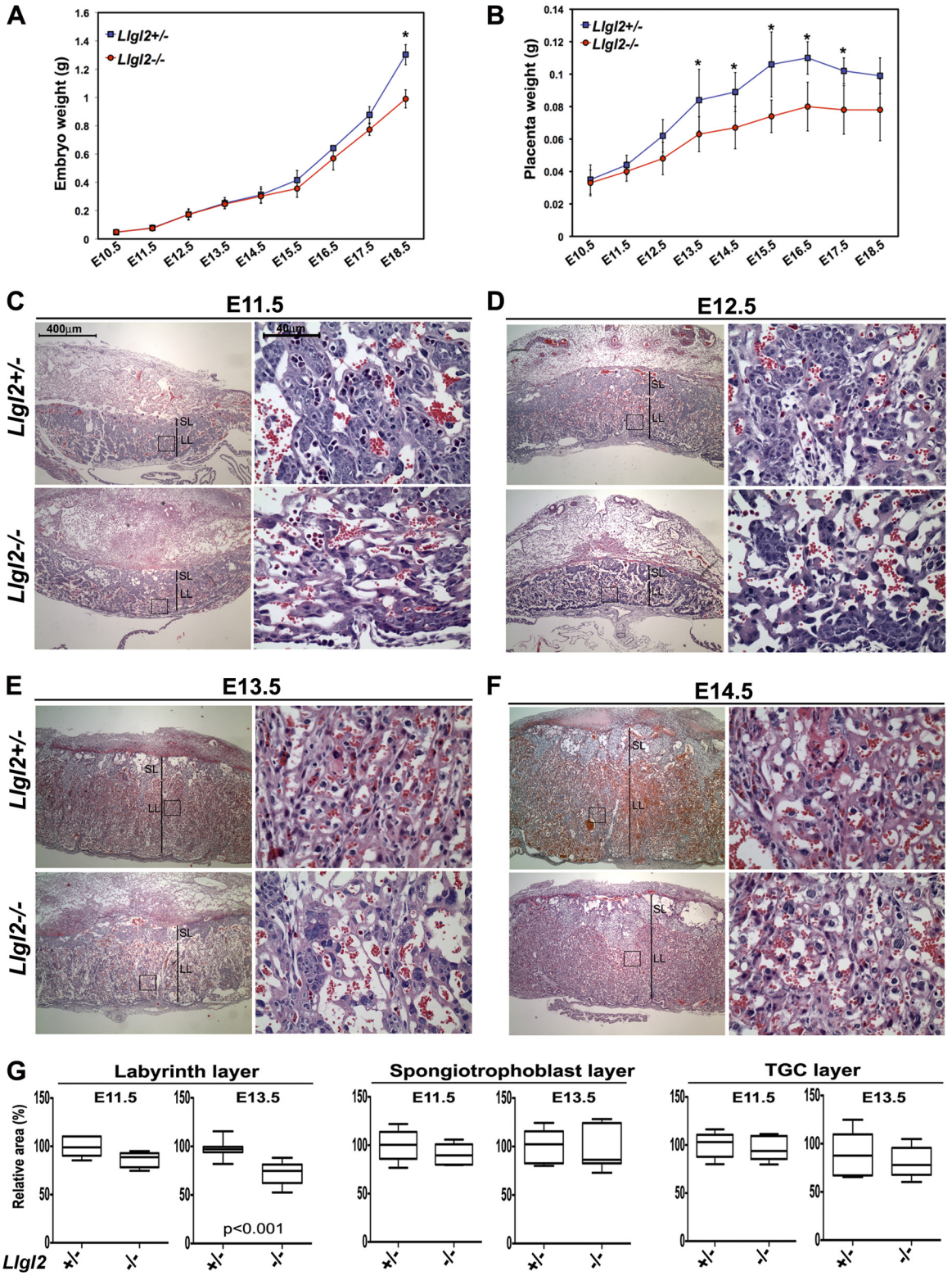

FIG. 3. *Llgl2* is required for proper placental morphogenesis. (A) Differences in weight between $Llgl2^{-/-}$ and $Llgl2^{+/-}$ embryos. Graph shows weights of the embryos at the indicated days of embryonic (E) development. Error bars represent standard deviations. Note that weight retardation of $Llgl2^{-/-}$ embryos becomes apparent at E15.5. *, $P < 0.01$. (B) Differences in weight between $Llgl2^{-/-}$ and $Llgl2^{+/-}$ placentas. Graph shows weights of the placentas at the indicated days of embryonic (E) development. Error bars represent standard deviations. Note that weight retardation of $Llgl2^{-/-}$ placentas becomes apparent at E12.5. *, $P < 0.01$. (C to F) Hematoxylin and eosin staining of sagittal sections through the central regions of E11.5 (C), E12.5 (D), E13.5 (E), and E14.5 (F) $Llgl2^{-/-}$ and $Llgl2^{+/-}$ placentas. The areas in squares are shown at higher magnification. SL, spongiotrophoblast layer; LL, labyrinth layer. Size bars for low- and high-magnification images in panels C to F are shown in panel C. (G) Quantitation of the relative sizes of the labyrinth, spongiotrophoblast, and trophoblast giant cell (TGC) layers in E11.5 and E13.5

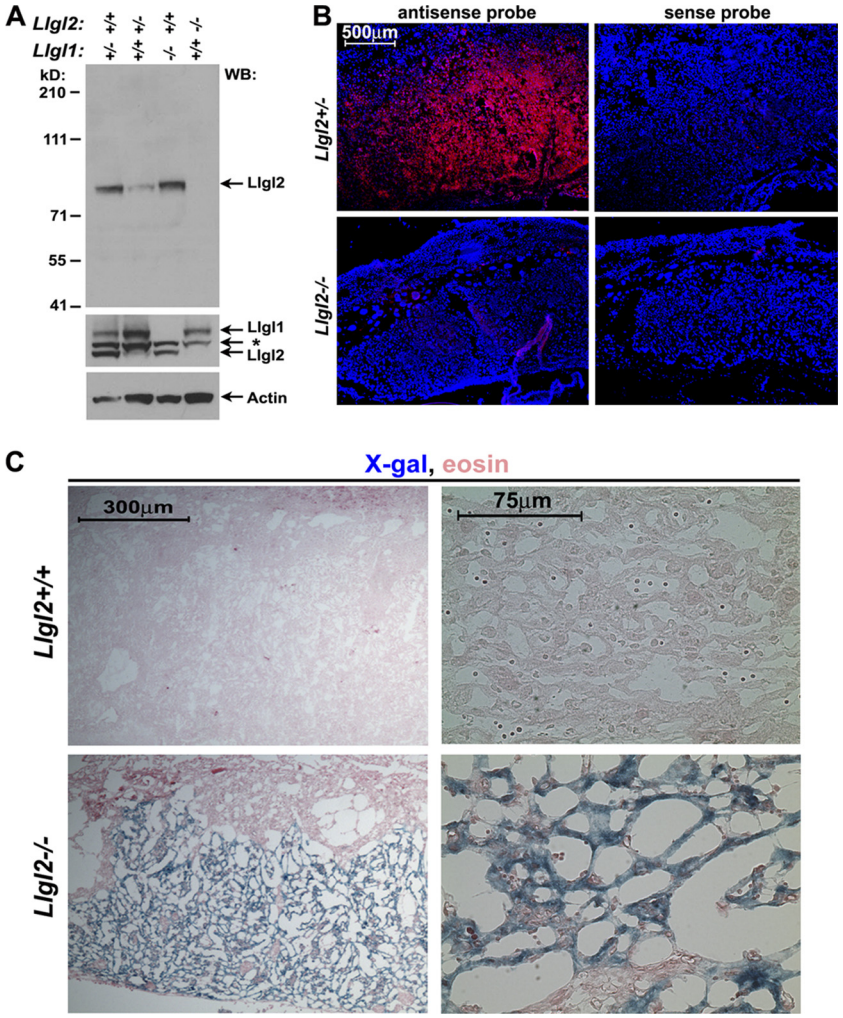

FIG. 4. *Llgl2* is prominently expressed in the placental labyrinth layer. (A) Western blot analyses of total protein extracts from *Llgl1*$^{-/-}$, *Llgl2*$^{-/-}$, and *Llgl2*$^{+/-}$ placentas with anti-Llgl2, anti-Llgl1, and anti-β-actin antibodies. Note that anti-Llgl1 antibodies weakly cross-react with Llgl2. Llgl1 is expressed at a low level in placenta, and the blot with anti-Llgl1 antibodies is overexposed. *, background band. (B) *In situ* hybridization of E13.5 *Llgl2*$^{-/-}$ and *Llgl2*$^{+/-}$ sagittal placental sections with antisense and sense (control) probes for *Llgl2* (red). Blue is a nuclear DAPI counterstain outlining general tissue morphology. Note the prominent expression of *Llgl2* in the placental labyrinth layer. (C) X-Gal staining of E13.5 *Llgl2*$^{+/+}$ and *Llgl2*$^{-/-}$ sagittal placental sections for β-geo activity. Note that while no staining was observed in wild-type placenta, trophoblasts of the labyrinth layer in *Llgl2*$^{-/-}$ placenta were prominently positive for β-geo activity.

the maternal and fetal blood. To reveal the primary defects in the *Llgl2*$^{-/-}$ labyrinth layer, we decided to analyze placentas by electron microscopy at E11.5, the earliest time point displaying the phenotype in mutant animals. These experiments revealed the presence of a well-defined trilaminar layer in both *Llgl2*$^{-/-}$ and *Llgl2*$^{+/-}$ placentas (Fig. 8C to E). The STI and STII layers were tightly apposed; however, they contained more frequent gaps and openings in *Llgl2*$^{-/-}$ placentas (Fig. 8D and E). Cell-cell junctions between STI and STII cell layers contain various cell-cell adhesion structures, which include desmosomes, gap junctions, and adherens junctions. Desmosomes were well visible at the level of electron microscopy, and we found no differences in desmosome formation between *Llgl2*$^{-/-}$ and *Llgl2*$^{+/-}$ placentas (Fig. 8D and E and data not shown). To analyze whether other cell-cell adhesion structures are lost or malformed in *Llgl2*$^{-/-}$ placentas, we performed stainings for markers of gap junctions (connexin 26) and adherens junctions (E-cadherin and β-catenin). No consistent

Llgl2$^{-/-}$ and *Llgl2*$^{+/-}$ placentas. The images of sagittal hematoxylin-and-eosin-stained sections through the central region of placentas were used to measure the relative area of each layer in pixels ($n = 6$). Box and whisker plots show areas in arbitrary units, with the area in control heterozygous placentas adjusted to 100%. Lines within boxes are median values. The upper and lower borders of the boxes represent 75th and 25th percentiles, respectively. The upper and lower bars represent maximum and minimum values. Statistical significance was assessed by the Mann-Whitney test, and *P* value is shown only for the data with statistically significant differences.

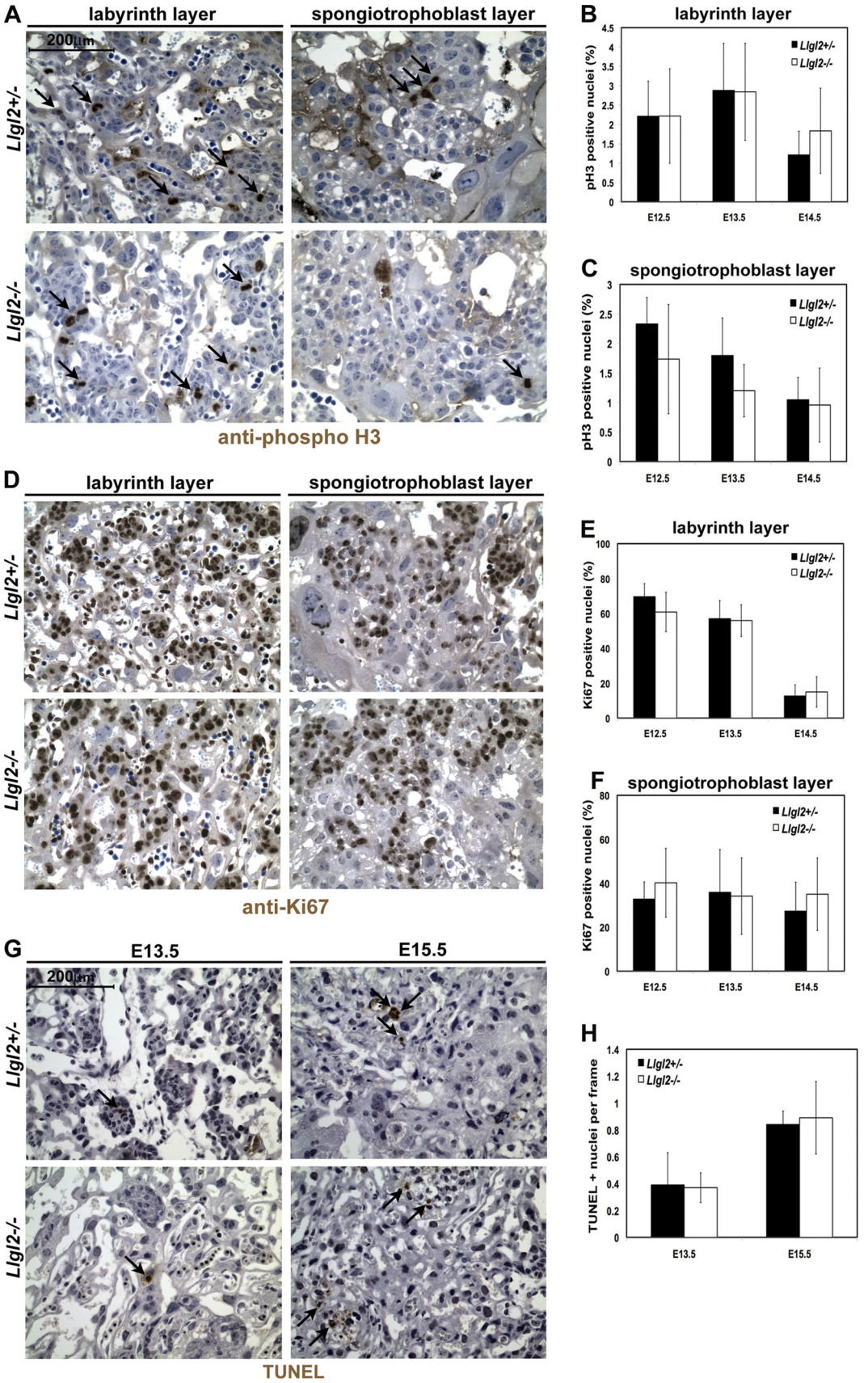
A
labyrinth layer
spongiotrophoblast layer
200μm
Lfgl2+/-
Lfgl2-/-
anti-phospho H3
B
labyrinth layer
pH3 positive nuclei (%)
Lfgl2+/-
Lfgl2-/-
E12.5
E13.5
E14.5
C
spongiotrophoblast layer
pH3 positive nuclei (%)
Lfgl2+/-
Lfgl2-/-
E12.5
E13.5
E14.5
D
labyrinth layer
spongiotrophoblast layer
Lfgl2+/-
Lfgl2-/-
anti-Ki67
E
labyrinth layer
Ki67 positive nuclei (%)
Lfgl2+/-
Lfgl2-/-
E12.5
E13.5
E14.5
F
spongiotrophoblast layer
Ki67 positive nuclei (%)
Lfgl2+/-
Lfgl2-/-
E12.5
E13.5
E14.5
G
E13.5
E15.5
200μm
Lfgl2+/-
Lfgl2-/-
TUNEL
H
TUNEL + nuclei per frame
Lfgl2+/-
Lfgl2-/-
E13.5
E15.5

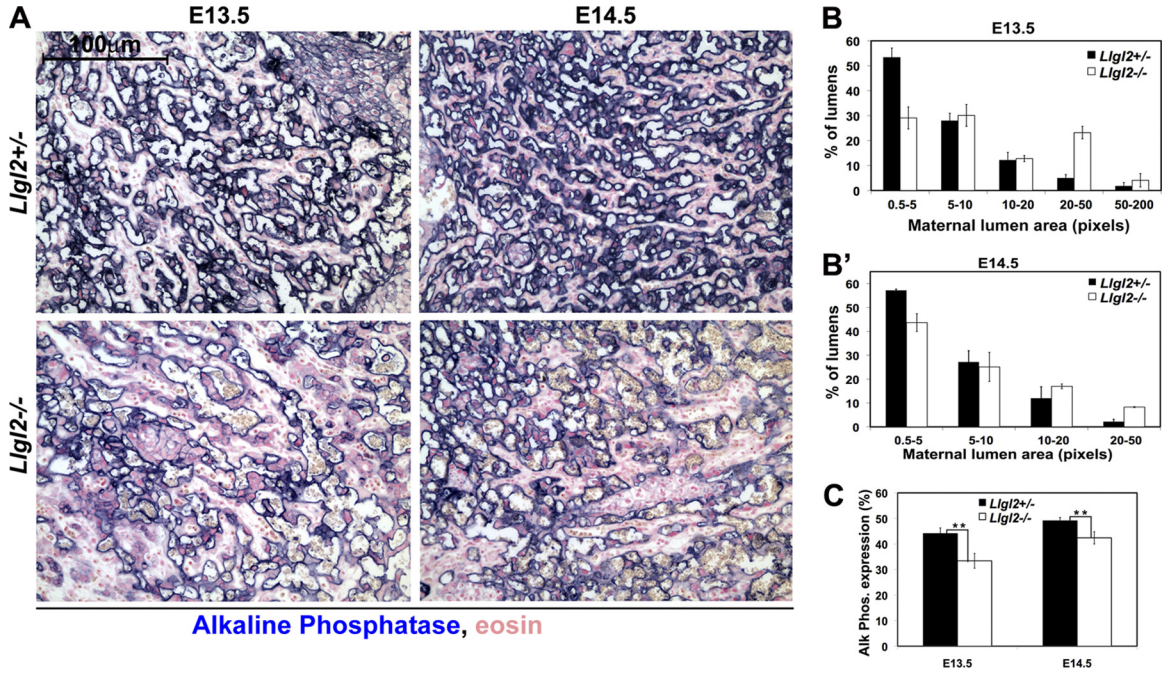

FIG. 6. Decreased branching and trophoblast transport surface area in *Llgl2*$^{-/-}$ placentas. (A) Alkaline phosphatase staining of sagittal sections through the central region of E13.5 and E14.5 *Llgl2*$^{-/-}$ and *Llgl2*$^{+/-}$ placentas. Maternal blood spaces in mouse placenta are lined with a syncytial trophoblast cell layer expressing endogenous alkaline phosphatase activity at the brash border. (B and B′) Image J software quantitation of sizes of maternal blood spaces at E13.5 (B) and E14.5 (B′) outlined by alkaline phosphatase staining shown in panel A. Bars represent the percentage of the lumens with indicated areas. Four randomly selected areas were quantified for each section ($n = 3$). The error bars represent standard deviations. Note the significant increase in the proportion of large (20 to 200 pixels) maternal blood lumens in *Llgl2*$^{-/-}$ placentas. (C) Morphometric analysis of the transport surface area outlined by alkaline phosphatase staining shown in panel A. The area of the alkaline phosphatase staining was digitized and the percentage of stained area on four randomly taken images of the labyrinth layer was quantified using Image J software as described previously (44). $n = 3$. *, $P < 0.01$.

differences were found in either the expression levels or the staining patterns of connexin 26, E-cadherin, and β-catenin between *Llgl2*$^{-/-}$ and *Llgl2*$^{+/-}$ placentas (Fig. 8F, G, and H). Since Llgl2 is believed to be a polarity protein involved in the establishment and maintenance of apical-basal cell polarity, we also performed stainings for cell polarity markers atypical PKC and Crumbs 3. Again, no differences were observed in the levels and staining pattern of these proteins (Fig. 8F, G, and H and data not shown). Overall, relatively normal formation of the trilaminar layer and the absence of discernible changes in localization of cell polarity markers indicate the absence of prominent steady-state cell polarity defects in *Llgl2*$^{-/-}$ placentas.

Expression of genes implicated in regulation of normal placental development does not change significantly in *Llgl2*$^{-/-}$ placentas. Many genes and signaling pathways have been implicated in mammalian placental development. To examine if these factors may be responsible for defective branching morphogenesis in *Llgl2*$^{-/-}$ placentas, we analyzed their expression using qRT-PCR (Fig. 9). We did not find significant differences in expression of *Hand1* and *Mash2* genes, which are required for trophoblast development and differentiation (Fig. 9) (16, 32). Similarly, expression of *Gcm1*, the gene critical for placental branching morphogenesis, and *Proliferin* (*Plf*), a prolactin family hormone stimulating placental angiogenesis, were also unchanged (Fig. 9) (2, 17). Expression levels of *SynA*, which is necessary for placental syncytiotrophoblast morphogenesis, were also unaffected (8). FGF10-FGFR2 signaling is important for proper placental branching morphogenesis (25, 45); however, we did not find changes in *Fgf10* expression levels in *Llgl2*$^{-/-}$ placentas (Fig. 9). Concordantly, the activities of MAPK and the Akt signaling pathway, which are the prominent targets of FGF signaling, were not significantly changed in *Llg2*$^{-/-}$ placentas (data not shown). Next, we an-

FIG. 5. Cell proliferation in *Llgl2*$^{-/-}$ and *Llgl2*$^{+/-}$ placentas. (A and D) Stainings of sagittal sections through the central regions of E12.5 *Llgl2*$^{-/-}$ and *Llgl2*$^{+/-}$ placentas with anti-phospho-histone H3 (mitotic cell marker) antibody (A) or anti-Ki67 antibody (proliferation marker) (D). Blue is a nuclear hematoxylin counterstain. (B, C, E, and F) Quantitation of stainings shown in panels A (B and C) and D (E and F). pH 3 and Ki67-positive nuclei were calculated as a percentage of the total number of nuclei on three randomly taken images from the labyrinth and spongiotrophoblast layers ($n = 3$ or greater). The error bars represent standard deviations. (G) TUNEL (apoptosis marker) staining of the labyrinth layers of *Llgl2*$^{-/-}$ and *Llgl2*$^{+/-}$ placentas at E13.5 and E15.5. (H) Quantitation of the stainings shown in panel G. The number of TUNEL-positive nuclei in at least 10 independent frames was counted for each section, and the number of TUNEL-positive nuclei per frame was calculated ($n = 3$). The error bars represent standard deviations.

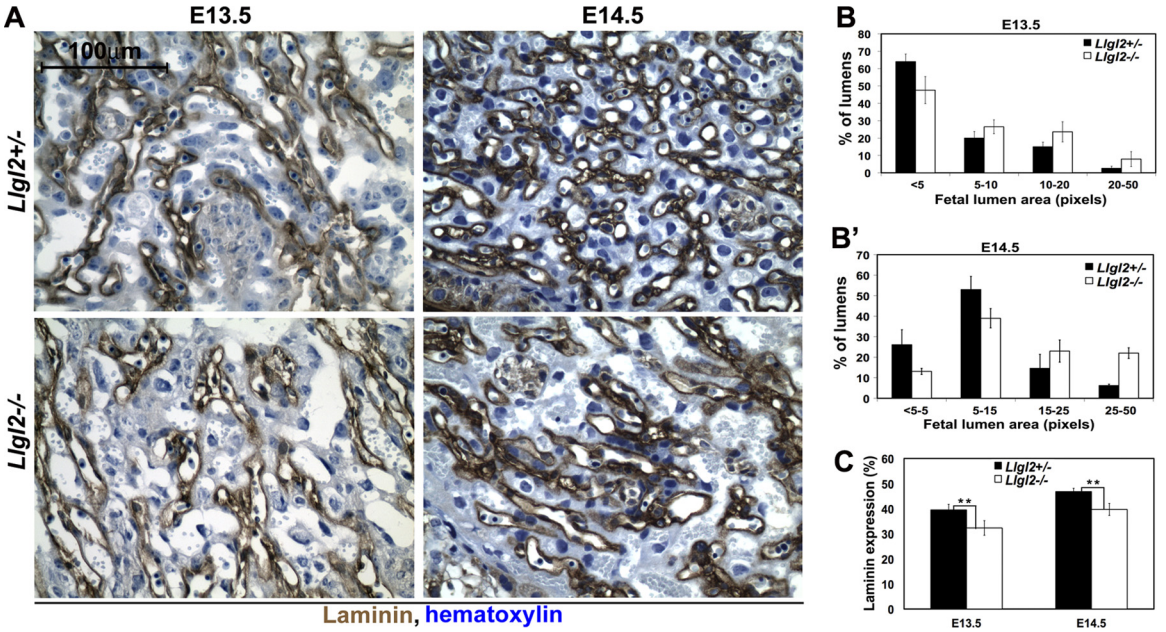

FIG. 7. Decreased vascularization in *Llgl2*$^{-/-}$ placentas. (A) Laminin staining of sagittal sections through the central region of E13.5 and E14.5 *Llgl2*$^{-/-}$ and *Llgl2*$^{+/-}$ placentas. Fetal blood spaces in mouse placenta are lined with a thin layer of endothelial cells residing on a prominent layer of laminin, which is detectable by staining with antilaminin antibodies. (B and B′) Image J software quantitation of sizes of fetal blood spaces at E13.5 (B) and E14.5 (B′) outlined by laminin staining shown in panel A. Bars represent the percentage of the lumens with indicated areas (n = 3). The error bars represent standard deviations. Note the increase in the proportion of large (5 to 50 pixels) fetal blood lumens in *Llgl2*$^{-/-}$ placentas. (C) Morphometric analysis of laminin-stained area. The area of the laminin staining was digitized and the percentage of stained area on four randomly taken images of the labyrinth layer was quantified using Image J software, as described previously (44). n = 3.

alyzed the expression levels of *Hey1* and *Hey2*, which are the endogenous targets of Notch signaling in placenta and are required for proper placental vasculogenesis (9). In addition to this, Lgl regulates Notch signaling in *Drosophila*, and *Llgl1*$^{-/-}$ embryos display increased Notch signaling in the developing brain (18). However, *Hey1* and *Hey2* expression levels remained unchanged in *Llgl2*$^{-/-}$ placentas, indicating that *Llgl2* does not impact the Notch signaling pathway in this organ (Fig. 9). Finally, qRT-PCR analysis of *Axin2*, an endogenous target of the canonical Wnt signaling pathway, also did not reveal changes in expression between *Llgl2*$^{-/-}$ and control placentas (Fig. 9) (48). We conclude that *Llgl2* is not a significant regulator of FGF, Notch, or Wnt signaling pathways in placental development and, therefore, these signaling pathways are unlikely to be responsible for the labyrinth phenotype in *Llgl2*$^{-/-}$ placentas.

***Llgl2* is necessary for induced polarization and directional invasion of placental trophoblasts.** Outgrowth of the labyrinth layer and branching morphogenesis of embryonic trophoblasts constitute a highly dynamic process, which is impossible to capture by the analysis of steady-state images from mutant placentas. To reveal the role of *Llgl2* in trophoblasts, we used the mouse placental labyrinthine trophoblast cell line SM10 (37, 38). Expression of *Llgl2* in these cells was knocked down (KD) using *Llgl2* lentiviral shRNA construct, and this knockdown was rescued by lentiviral reexpression of human V5-tagged LLGL2 (Fig. 10A and B). We used these cells to analyze the potential role of *Llgl2* in the regulation of trophoblast migration, invasion, and induced polarization.

Migration and invasion of placental trophoblasts play a critical role in placental development. We found significant differences in the rates of cell migration and Matrigel invasion between Llgl2KD and control cells (Fig. 10C, E, and F). The cultured placental trophoblasts are invasive in Matrigel invasion assays. Llgl2KD cells displayed significantly decreased rates of Matrigel invasion, and these differences were rescued by reexpression of human LLGL2 (Fig. 10C). Expression of extracellular matrix metalloproteinases (MMPs) plays a critical role in Matrigel invasion (39, 42). We analyzed the activity of MMPs using zymogram assays; however, no differences in MMP activities were observed between Llgl2KD and control cells (Fig. 10D). In addition to the defects in Matrigel invasion, Llgl2KD cells displayed significantly reduced rates of migration in short-term transwell migration assays (Fig. 10E). These differences disappear after long-term exposure, when cells have had enough time to equilibrate between the inner and outer surfaces of the transwell membrane (Fig. 10F). These data indicate that *Llgl2* is not required for cell migration *per se* but is necessary for directional cell migration and invasion.

The ability of cells to polarize in response to stimuli plays a critical role in regulation of directional cell migration and invasion. We hypothesized that *Llgl2* may be required for timely cell polarization and reorientation toward a stimulus, and the failure of cells to polarize may be responsible for the defects in invasion and short-term migration observed in Llgl2KD cells. To address this issue, we performed scratch wound cell polarization assays (36). We found that within 1 h after monolayer wounding, 68% of control cells polarized toward the wound (Fig. 10G and H). In contrast, only 40% of Llgl2KD cells were polarized. Importantly, these differences in

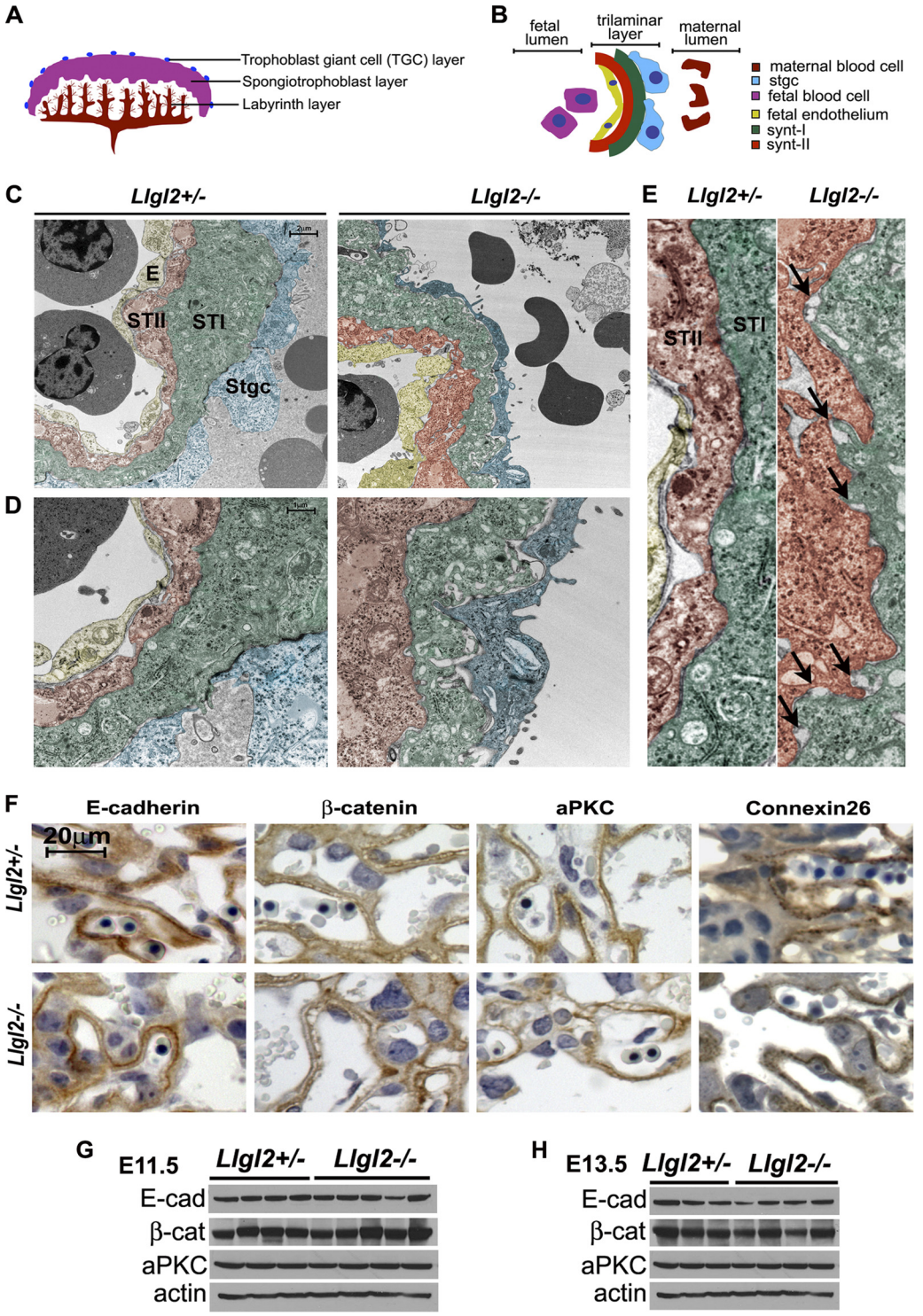

FIG. 8. Trilaminar cell layer and markers of cell adhesion and cell polarity in *Lgl2*$^{-/-}$ and *Lgl2*$^{+/-}$ placentas. (A and B) Schematic representation of mouse placenta (A) and trilaminar cell layer separating maternal and embryonic blood spaces (B). (C to E) Pseudocolored electron micrographs from the labyrinth layers of E11.5 *Lgl2*$^{-/-}$ and *Lgl2*$^{+/-}$ placentas. The three layered interhemal barrier at the maternofetal interface indicates the maternal (enucleated) and fetal blood cells (nucleated) separated by the endothelium (E) that lines fetal lumen and two syncytiotrophoblast layers (ST-I and ST-II). Mononuclear sinusoidal giant trophoblast cells (Sgtc) are seen associated with the ST-I cell layer (scale bar, 2 μm). Images are shown at low (C), intermediate (D), and high (E) magnifications. Arrows in panel E show small areas of membrane separation between ST-I and ST-II cell layers in *Lgl2*$^{-/-}$ placentas. The scale bar in panel C corresponds to 2 μm in panel C, 1 μm in panel D, and 0.5 μm in panel E. (F) Immunohistochemical stainings of sagittal placental sections through the central region of E13.5 *Lgl2*$^{-/-}$ and *Lgl2*$^{+/-}$ placentas with anti-E-cadherin, anti-β-catenin, anti-atypical PKC, and anti-connexin 26 antibodies (22). Blue is hematoxylin counterstain. (G and H) Western blot analysis of total protein extracts from E11.5 (G) and E13.5 (H) *Lgl2*$^{-/-}$ and *Lgl2*$^{+/-}$ placentas with anti-E-cadherin (E-cad), anti-β-catenin (β-cat), anti-atypical PKC zeta (aPKC), and anti-β-actin antibodies.

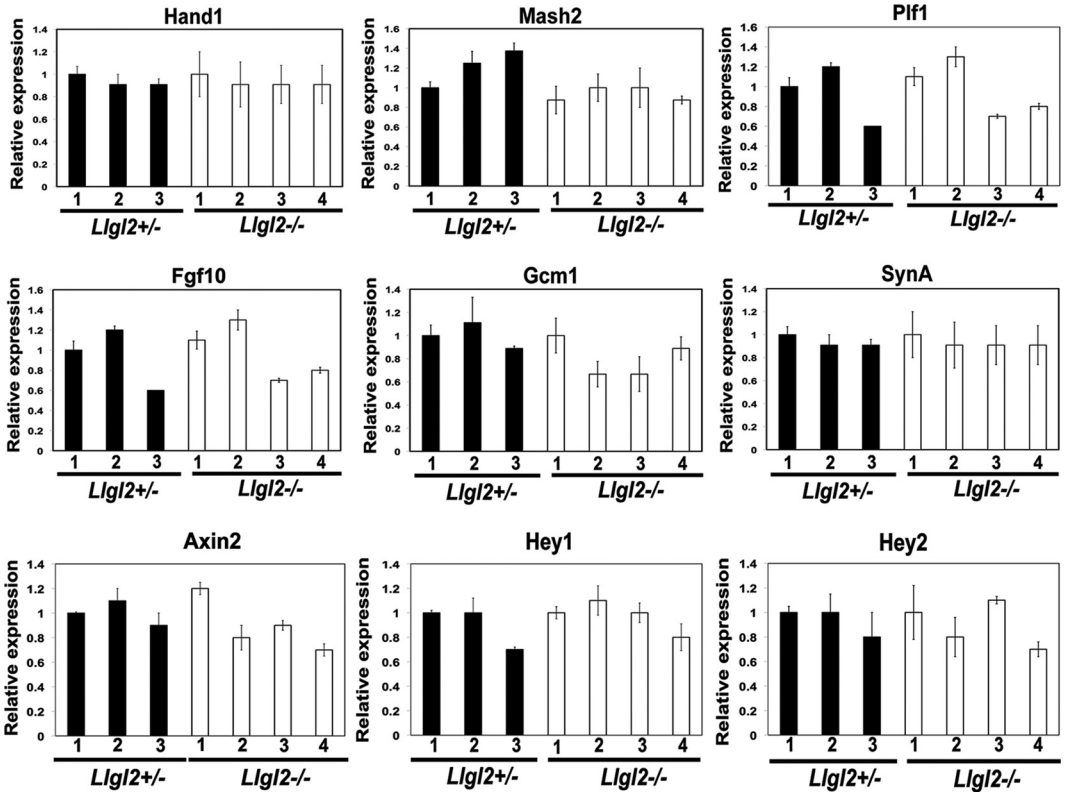

FIG. 9. Expression levels of genes implicated in regulation of normal placental development in *Llgl2*$^{+/-}$ and *Llgl2*$^{-/-}$ placentas. Total RNA was extracted from E11.5 *Llgl2*$^{-/-}$ and *Llgl2*$^{+/-}$ placentas, and the expression levels of indicated genes were analyzed by qRT-PCR. Ribosomal *Rsp16* was used as a normalization control. Bar graphs show mean values for three *Llgl2*$^{+/-}$ and four *Llgl2*$^{-/-}$ placentas ± standard deviation (SD). In each case, expression level in the first *Llgl2*$^{+/-}$ sample was arbitrarily adjusted to 1.

induced cell polarization were rescued by reexpression of human LLGL2 (Fig. 10G and H). We conclude that *Llgl2* is required for dynamic repolarization of placental trophoblasts. The deficiency in the ability of cells to polarize in a timely manner may be responsible for the decreased rates of branching morphogenesis in *Llgl2*$^{-/-}$ placenta.

DISCUSSION

Lgl is an important apical-basal cell polarity gene in *Drosophila*. To reveal the *in vivo* role of mammalian orthologs of *Drosophila Lgl*, we generated and analyzed mouse mutants for *Llgl1* and *Llgl2*. We previously reported that *Llgl1*$^{-/-}$ mice display a prominent brain phenotype and show disruption of cell polarity in neural progenitor cells (18). We report here that *Llgl2*$^{-/-}$ mice display a very specific defect in placental development and show that *Llgl2* is required for branching morphogenesis of the placental labyrinth layer.

While *Llgl2* is necessary for proper placental development, it is not required either in the developing embryo or in the adult mice. The lack of significant abnormalities in *Llgl2*$^{-/-}$ mice is a surprising finding of this study. Indeed, the mutation of *Lgl2* in zebrafish results in a dramatic phenotype in embryonic epidermis, which shows a loss of hemidesmosomes and displays prominent hyperproliferation (40, 41). Moreover, *Lgl2* overexpression experiments in *Xenopus* suggested an important role for Lgl2 in the maintenance of cell polarity of early blastomeres and in proper regulation of neurogenesis (6, 34). Our results indicate that *Llgl2* serves a nonessential or redundant function in mice. We believe that its function is more likely to be redundant, since a closely related mouse homolog of *Llgl2*, *Llgl1*, is prominently expressed in all mouse organs and may compensate for the loss of *Llgl2*. Indeed, the phenotype in *Llgl1*$^{-/-}$ mice is restricted to the developing brain, which is the only developing organ where *Llgl2* is not expressed and, hence, cannot compensate for the loss of *Llgl1* (18). Moreover, the cell polarity phenotype in MDCK cells and the mitotic spindle disorganization phenotype in HEK293 cells are exhibited only when both *Llgl1* and *Llgl2* genes are simultaneously knocked down (46). These findings suggest that *Llgl1* and *Llgl2* are likely to play a redundant role and the lack of the prominent phenotype in *Llgl2*$^{-/-}$ mice is due to compensation by *Llgl1*. Interestingly, we found that Llgl1 is also expressed in placenta, and, therefore, the placental phenotype in our *Llgl2*$^{-/-}$ animals cannot be explained by the absence of *Llgl1* expression in this organ. One possibility is that the overall levels of Llgl proteins are important for normal placental development and depletion of Llgl2 results in a placental phenotype, which may become even more dramatic in double-mutant *Llgl1*/*Llgl2* embryos. Future generation and analysis of *Llgl1*/*Llgl2* double mutant mice will be informative for understanding the *in vivo* function of mouse Llgl proteins.

Llgl2$^{-/-}$ mice display a very specific defect in branching morphogenesis of the placental labyrinth layer. Many genes

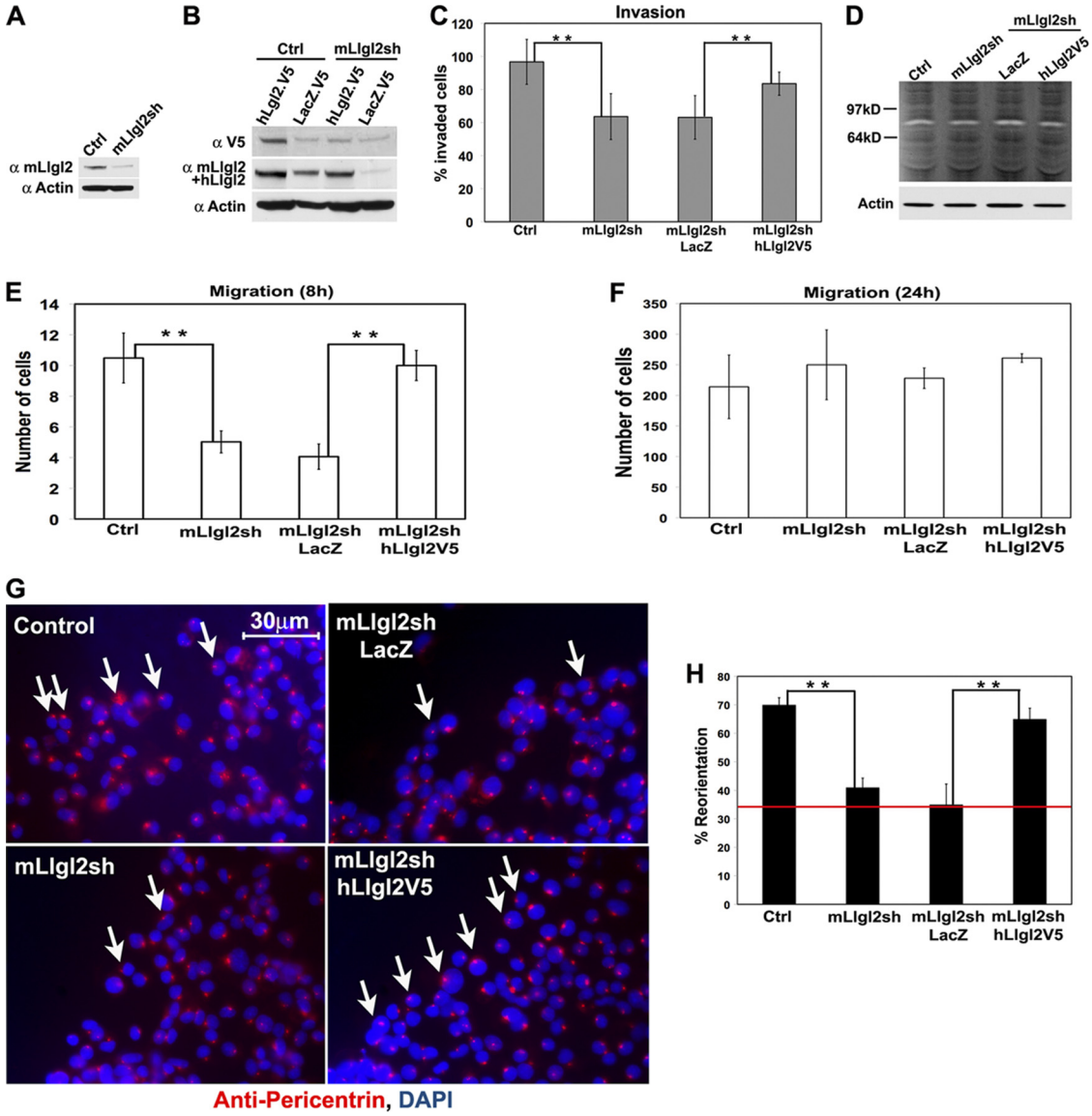

FIG. 10. Llgl2 is necessary for induced polarization and polarized migration and invasion of placental trophoblasts. (A and B) Western blot analyses of total protein extracts from SM10 trophoblast cells stably transduced with lentiviral control (Ctrl) or mouse *Llgl2*-targeting (mLlgl2sh) shRNAs and expressing LacZ (LacZ.V5) or human LLGL2 (hLlgl2.V5) proteins. Proteins analyzed with anti-V5 (α V5), anti-mouse or -human Llgl2 (α mLlgl2+hLlgl2), and anti-β-actin (α Actin) antibodies. (C) Quantitation of Matrigel cell invasion assays of SM10 cells transduced with lentiviral control (Ctrl) or mouse *Llgl2*-targeting (mLlgl2sh) shRNAs and expressing LacZ or human LLGL2 (hLlgl2V5). Bar graph shows mean values of invaded cells ± standard deviation (SD). **, $P < 0.01$. (D) Protease zymography of SM10 cells transduced with lentiviral control (Ctrl) or mouse *Llgl2*-targeting (mLlgl2sh) shRNAs and expressing LacZ or human LLGL2 (hLlgl2V5). Total cell proteins were separated on gelatin gels, renatured, exposed to gelatin substrate, and stained by Coomassie. Clear bands indicate position and activity of gelatinases. Proteins were analyzed in parallel by Western blotting with anti-β-actin (Actin) antibodies. (E and F) Quantitation of short-term (E, 8 h) and long-term (F, 24 h) transwell cell migration assays of SM10 cells transduced with lentiviral control (Ctrl) or mouse *Llgl2*-targeting (mLlgl2sh) shRNAs and expressing LacZ or human LLGL2 (hLlgl2V5). Bar graph shows mean values of migrated cells ± SD. **, $P < 0.01$. (G) Centrosome reorientation toward the scratch wound in SM10 cells transduced with lentiviral control (Ctrl) or mouse *Llgl2*-targeting (mLlgl2sh) shRNAs and expressing LacZ or human LLGL2 (hLlgl2V5) at 1 h after wounding. Immunofluorescent staining of the wound edge with antipericentrin antibodies (red). DAPI is a nuclear counterstain (blue). Arrows point to cells properly oriented toward the scratch wound. (H) Quantitation of centrosome reorientation shown in panel G. The graph shows mean values ± SD of centrosomes polarized toward the wound cells. $n \geq 150$. **, $P < 0.01$. Red line shows the value for random orientation of centrosomes.

and signaling pathways have been implicated in regulation of proper placenta development (43). The phenotypes of mouse mutants with placental defects vary tremendously. The most severely affected mutants display a compacted labyrinth layer with very little branching, usually resulting in embryonic lethality (3, 8, 13, 43, 47). In contrast, partial deficiency in the branching of the labyrinth layer leads to undersized newborns which either die postnatally or, similarly to *Llgl2*$^{-/-}$ pups, survive to be normal adults (20, 33, 35, 45). qRT-PCR analyses of the expression levels of many genes critical for placental

development failed to reveal consistent differences between heterozygous and *Llgl2*$^{-/-}$ placentas. Instead, we found a specific defect in the ability of placental trophoblasts to repolarize in response to stimuli.

Our work reveals an important role of mammalian *Llgl2* in cell polarity, and this is consistent with the notion of *Lgls* as cell polarity genes in other model organisms. Since we did not observe steady-state cell polarity defects in *Llgl2*$^{-/-}$ placentas, it is likely that the *Llgl2* function in cell polarity is somewhat redundant even in the placenta and that the requirement of Llgl2 is revealed only when cells have to quickly repolarize in response to the modified external cues. The ability to quickly readjust the cell polarity axis is likely to play a very important role during the highly dynamic process of branching morphogenesis, which is associated with rapid remodeling of cell-cell and cell-substratum adhesion junctions. Therefore, it is possible that the inability to promptly respond to very dynamic and ever-changing cell polarization cues can cause the general decrease in placental branching morphogenesis in *Llgl2*$^{-/-}$ embryos.

Branching morphogenesis is one of the fundamental processes employed by the developing embryo to increase the surface area of an organ. In addition to placental development, this morphogenetic event plays an important role in the development of lung, kidney, pancreas, vasculature, breast, prostate, and salivary glands. Despite its important role in metazoan development, the mechanisms responsible for branching morphogenesis are not well understood, and it is an active area of recent research (24, 28). Since *Llgl2* is one of the canonical apical-basal cell polarity genes, our data suggest that apical-basal cell polarity mechanisms may play an important role in the regulation of mammalian branching morphogenesis. Future analysis of *Llgl1*/*Llgl2* double-mutant mice will help to determine whether Lgl proteins are necessary for branching morphogenesis in other organs of the developing mammalian embryo.

ACKNOWLEDGMENTS

We thank all members of our laboratory for suggestions and comments, Nanyan Jiang for blastocyst injection of ES cells, Olga Klezovitch for help with the maintenance of mutant mice, and William Carter, Paul Lampe, and the Developmental Studies Hybridoma Bank for gifts of antibodies.

This work was supported by NCI grants R01 CA098161 and R01 CA131047 to V.V.

REFERENCES

1. **Adamson, S. L., et al.** 2002. Interactions between trophoblast cells and the maternal and fetal circulation in the mouse placenta. Dev. Biol. **250:**358–373.
2. **Anson-Cartwright, L., et al.** 2000. The glial cells missing-1 protein is essential for branching morphogenesis in the chorioallantoic placenta. Nat. Genet. **25:**311–314.
3. **Barak, Y., et al.** 1999. PPAR gamma is required for placental, cardiac, and adipose tissue development. Mol. Cell **4:**585–595.
4. **Bilder, D.** 2004. Epithelial polarity and proliferation control: links from the Drosophila neoplastic tumor suppressors. Genes Dev. **18:**1909–1925.
5. **Bilder, D., M. Li, and N. Perrimon.** 2000. Cooperative regulation of cell polarity and growth by Drosophila tumor suppressors. Science **289:**113–116.
6. **Chalmers, A. D., et al.** 2005. aPKC, Crumbs3 and Lgl2 control apicobasal polarity in early vertebrate development. Development **132:**977–986.
7. **Dowling, J., Q. C. Yu, and E. Fuchs.** 1996. Beta4 integrin is required for hemidesmosome formation, cell adhesion and cell survival. J. Cell Biol. **134:**559–572.
8. **Dupressoir, A., et al.** 2009. Syncytin-A knockout mice demonstrate the critical role in placentation of a fusogenic, endogenous retrovirus-derived, envelope gene. Proc. Natl. Acad. Sci. U. S. A. **106:**12127–12132.
9. **Fischer, A., N. Schumacher, M. Maier, M. Sendtner, and M. Gessler.** 2004. The Notch target genes Hey1 and Hey2 are required for embryonic vascular development. Genes Dev. **18:**901–911.
10. **Gateff, E.** 1978. The genetics and epigenetics of neoplasms in Drosophila. Biol. Rev. Camb. Philos. Soc. **53:**123–168.
11. **Gateff, E.** 1978. Malignant neoplasms of genetic origin in Drosophila melanogaster. Science **200:**1448–1459.
12. **Gateff, E., and H. A. Schneiderman.** 1969. Neoplasms in mutant and cultured wild-tupe tissues of Drosophila. Natl. Cancer Inst. Monogr. **31:**365–397.
13. **Giroux, S., et al.** 1999. Embryonic death of Mek1-deficient mice reveals a role for this kinase in angiogenesis in the labyrinthine region of the placenta. Curr. Biol. **9:**369–372.
14. **Grifoni, D., et al.** 2007. aPKCzeta cortical loading is associated with Lgl cytoplasmic release and tumor growth in Drosophila and human epithelia. Oncogene **26:**5960–5965.
15. **Grifoni, D., et al.** 2004. The human protein Hugl-1 substitutes for Drosophila lethal giant larvae tumour suppressor function in vivo. Oncogene **23:**8688–8694.
16. **Guillemot, F., et al.** 1995. Genomic imprinting of Mash2, a mouse gene required for trophoblast development. Nat. Genet. **9:**235–242.

16a. **Hogan, B., R. Beddington, F. Costantini, and E. Lacy.** 1994. Manipulating the mouse embryo. A laboratory manual, 2nd ed. Cold Spring Harbor Laboratory Press, Cold Spring Harbor, NY.

17. **Jackson, D., O. V. Volpert, N. Bouck, and D. I. Linzer.** 1994. Stimulation and inhibition of angiogenesis by placental proliferin and proliferin-related protein. Science **266:**1581–1584.
18. **Klezovitch, O., T. E. Fernandez, S. J. Tapscott, and V. Vasioukhin.** 2004. Loss of cell polarity causes severe brain dysplasia in Lgl1 knockout mice. Genes Dev. **18:**559–571.
19. **Lee, M., and V. Vasioukhin.** 2008. Cell polarity and cancer—cell and tissue polarity as a non-canonical tumor suppressor. J. Cell Sci. **121:**1141–1150.
20. **Li, Y., and R. R. Behringer.** 1998. Esx1 is an X-chromosome-imprinted regulator of placental development and fetal growth. Nat. Genet. **20:**309–311.
21. **Lien, W.-H., V. I. Gelfand, and V. Vasioukhin.** 2008. αE-catenin binds to dynamitin and regulates dynactin-mediated intracellular traffic. J. Cell Biol. **183:**989–997.
22. **Lois, C., E. J. Hong, S. Pease, E. J. Brown, and D. Baltimore.** 2002. Germline transmission and tissue-specific expression of transgenes delivered by lentiviral vectors. Science **295:**868–872.
23. **Mechler, B. M., W. McGinnis, and W. J. Gehring.** 1985. Molecular cloning of lethal(2)giant larvae, a recessive oncogene of Drosophila melanogaster. EMBO J. **4:**1551–1557.
24. **Metzger, R. J., O. D. Klein, G. R. Martin, and M. A. Krasnow.** 2008. The branching programme of mouse lung development. Nature **453:**745–750.
25. **Natanson-Yaron, S., et al.** 2007. FGF 10 and Sprouty 2 modulate trophoblast invasion and branching morphogenesis. Mol. Hum. Reprod. **13:**511–519.
26. **Neumuller, R. A., and J. A. Knoblich.** 2009. Dividing cellular asymmetry: asymmetric cell division and its implications for stem cells and cancer. Genes Dev. **23:**2675–2699.
27. **Ohshiro, T., T. Yagami, C. Zhang, and F. Matsuzaki.** 2000. Role of cortical tumour-suppressor proteins in asymmetric division of Drosophila neuroblast. Nature **408:**593–596.
28. **Onodera, T., et al.** 2010. Btbd7 regulates epithelial cell dynamics and branching morphogenesis. Science **329:**562–565.
29. **Peng, C. Y., L. Manning, R. Albertson, and C. Q. Doe.** 2000. The tumour-suppressor genes lgl and dlg regulate basal protein targeting in Drosophila neuroblasts. Nature **408:**596–600.
30. **Prehoda, K. E.** 2009. Polarization of Drosophila neuroblasts during asymmetric division. Cold Spring Harb. Perspect. Biol. **1:**a001388
31. **Reischauer, S., M. P. Levesque, C. Nusslein-Volhard, and M. Sonawane.** 2009. Lgl2 executes its function as a tumor suppressor by regulating ErbB signaling in the zebrafish epidermis. PLoS Genet. **5:**e1000720.
32. **Riley, P., L. Anson-Cartwright, and J. C. Cross.** 1998. The Hand1 bHLH transcription factor is essential for placentation and cardiac morphogenesis. Nat. Genet. **18:**271–275.
33. **Rodriguez, T. A., et al.** 2004. Cited1 is required in trophoblasts for placental development and for embryo growth and survival. Mol. Cell. Biol. **24:**228–244.
34. **Sabherwal, N., et al.** 2009. The apicobasal polarity kinase aPKC functions as a nuclear determinant and regulates cell proliferation and fate during Xenopus primary neurogenesis. Development **136:**2767–2777.
35. **Saxton, T. M., et al.** 2001. Gene dosage-dependent functions for phosphotyrosine-Grb2 signaling during mammalian tissue morphogenesis. Curr. Biol. **11:**662–670.
36. **Schlessinger, K., E. J. McManus, and A. Hall.** 2007. Cdc42 and noncanonical Wnt signal transduction pathways cooperate to promote cell polarity. J. Cell Biol. **178:**355–361.
37. **Sharma, R. K.** 1998. Mouse trophoblastic cell lines. I: relationship between invasive potential and TGF-beta 1. In Vivo **12:**431–440.
38. **Sharma, R. K.** 1998. Mouse trophoblastic cell lines. II: relationship between invasive potential and proteases. In Vivo **12:**209–217.

39. **Solberg, H., J. Rinkenberger, K. Dano, Z. Werb, and L. R. Lund.** 2003. A functional overlap of plasminogen and MMPs regulates vascularization during placental development. Development **130:**4439–4450.
40. **Sonawane, M., et al.** 2005. Zebrafish penner/lethal giant larvae 2 functions in hemidesmosome formation, maintenance of cellular morphology and growth regulation in the developing basal epidermis. Development **132:**3255–3265.
41. **Sonawane, M., H. Martin-Maischein, H. Schwarz, and C. Nusslein-Volhard.** 2009. Lgl2 and E-cadherin act antagonistically to regulate hemidesmosome formation during epidermal development in zebrafish. Development **136:** 1231–1240.
42. **Teesalu, T., R. Masson, P. Basset, F. Blasi, and D. Talarico.** 1999. Expression of matrix metalloproteinases during murine chorioallantoic placenta maturation. Dev. Dyn. **214:**248–258.
43. **Watson, E. D., and J. C. Cross.** 2005. Development of structures and transport functions in the mouse placenta. Physiology (Bethesda) **20:**180–193.
44. **Wu, L., et al.** 2003. Extra-embryonic function of Rb is essential for embryonic development and viability. Nature **421:**942–947.
45. **Xu, X., et al.** 1998. Fibroblast growth factor receptor 2 (FGFR2)-mediated reciprocal regulation loop between FGF8 and FGF10 is essential for limb induction. Development **125:**753–765.
46. **Yamanaka, T., et al.** 2006. Lgl mediates apical domain disassembly by suppressing the PAR-3-aPKC-PAR-6 complex to orient apical membrane polarity. J. Cell Sci. **119:**2107–2118.
47. **Yan, L., et al.** 2003. Knockout of ERK5 causes multiple defects in placental and embryonic development. BMC Dev. Biol. **3:**11.
48. **Yu, H. M., et al.** 2005. The role of Axin2 in calvarial morphogenesis and craniosynostosis. Development **132:**1995–2005.